# Segmentation of Heterochromatin Foci Using a 3D Spherical Harmonics Intensity Model

Simon Eck[1], Stefan Wörz[1], Andreas Biesdorf[1], Katharina Müller-Ott[2], Karsten Rippe[2], and Karl Rohr[1]

[1]University of Heidelberg, BIOQUANT, IPMB, and DKFZ Heidelberg,
Dept. Bioinformatics and Functional Genomics, Biomedical Computer Vision Group
Im Neuenheimer Feld 267, 69120 Heidelberg, Germany
[2]DKFZ Heidelberg and BIOQUANT,
Research Group Genome Organization & Function
`simon.eck@bioquant.uni-heidelberg.de`

**Abstract.** We introduce a 3D model-based approach for automatic segmentation of 3D fluorescent heterochromatin foci from 3D microscopy images. The approach employs a new 3D parametric intensity model based on a spherical harmonics (SH) expansion and can represent foci of regular and highly irregular shapes. By solving a least-squares optimization problem, the model is directly fitted to the 3D image data, and the model parameters including the SH expansion coefficients are estimated. The approach has been successfully applied to real 3D microscopy image data. A visual comparison and a quantitative evaluation show that the new approach yields better results than previous approaches.

## 1 Introduction

The analysis of heterochromatin structures and heterochromatin associated proteins from 3D microscopy image data is important to study genome regulation and cell function. Using confocal light microscopy, these structures can be visualized as *fluorescent foci*. Since biological studies often involve large amounts of 3D microscopy image data, manual image analysis is not feasible. Moreover, the size, 3D shape, and signal intensity of the foci can vary significantly (see Fig. 1). Hence, a robust automatic image analysis approach is required which can cope well with *highly irregular shapes* even in the case of high noise.

Previous approaches for segmentation of heterochromatin structures from microscopy images often rely on global intensity thresholds (e.g., [1]). In [2], segmentation is performed by energy minimization within image regions. However, the aforementioned approaches are bound to the pixel raster and do not obtain an analytic representation of the foci. In contrast, model-based approaches, e.g., based on parametric intensity models, are not bound to the pixel raster and allow determining an analytic representation. 3D parametric intensity models have successfully been used for 3D segmentation of subcellular structures from microscopy images (e.g., [3,4]) and for heterochromatin analysis [5]. However, there only regularly shaped models (e.g., ellipsoids) were used.

In this work, we propose an automatic approach for 3D model-based segmentation of fluorescent foci from heterochromatin microscopy images. We introduce a new 3D parametric intensity model based on *spherical harmonics* (SH), which in comparison to [3,4,5] copes well with highly irregular foci shapes. SH form a complete orthogonal set of basis functions, enabling spherical functions to be expanded into a series of SH [6,7]. In biomedical image analysis, SH were previously used, e.g., for shape characterization [8], shape registration [9], and surface smoothing. However, only few approaches *directly* employ SH for model-based *segmentation* [6,10]. So far, such approaches were not used for microscopy images and they require training data [6] or manual initialization [10]. In our approach, training data is not necessary and the proposed 3D SH intensity model is initialized fully automatically. By solving a least-squares optimization problem, the model is directly fitted to the image data. The new approach has been successfully applied to real 3D microscopy images.

## 2  Materials and Methods

### 2.1  Spherical Harmonics Expansion

In our approach, we analytically describe the 3D shape of fluorescent foci using a *spherical harmonics* (SH) expansion. SH form a complete set of basis functions defined on the sphere, enabling spherical functions to be expanded into a series of weighted SH [6,7]. The real-valued SH of *degree l* and *order m* are defined by

$$Y_l^m(\theta, \varphi) = \begin{cases} \sqrt{2} N_l^m P_l^m(\cos\theta) \cos(m\varphi) & m > 0 \\ N_l^0 P_l^0(\cos\theta) & m = 0 \\ \sqrt{2} N_l^{|m|} P_l^{|m|}(\cos\theta) \sin(|m|\varphi) & m < 0 \end{cases} \tag{1}$$

where $P_l^m$ is an associated Legendre polynomial. The normalization coefficients $N_l^m = \sqrt{\frac{2l+1}{4\pi} \frac{(l-m)!}{(l+m)!}}$ are chosen such that $Y_l^m$ are orthonormal [7]. To describe
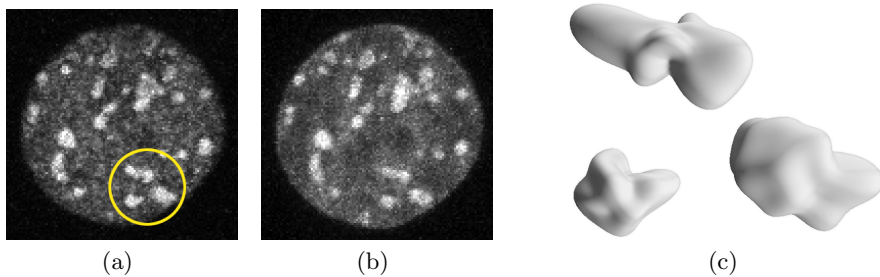


**Fig. 1.** Maximum intensity projections (MIPs) of a cell nucleus in a 3D two-channel fluorescence microscopy image: Heterochromatin protein 1$\alpha$ (a) and heterochromatin (b). (c) 3D segmentation results of the irregularly shaped foci marked in (a).

the shape of fluorescent foci using a series of SH, we assume the foci to be star-shaped. Let $F$ denote the 3D region of a fluorescent focus, then $F$ is said to be *star-shaped*, if a point $\mathbf{q} \in F$ exists such that each ray originating from $\mathbf{q}$ intersects the surface of $F$ exactly once. If $\mathbf{q}$ is the origin of a spherical coordinate system, then the surface of $F$ can be represented by a 3D radius function $r(\theta, \varphi)$, where $\theta \in [0, \pi]$ and $\varphi \in [0, 2\pi)$ are the inclination and azimuth angles, respectively. Based on (1), the real-valued SH expansion for approximation of $r(\theta, \varphi)$ can be stated as

$$r_{\mathrm{SH}} = \sum_{l=0}^{l_{\max}} \left[ a_l^0 N_l^0 P_l^0(\cos\theta) + \sum_{m=1}^{l} \left[ a_l^m \cos(m\varphi) + b_l^m \sin(m\varphi) \right] \sqrt{2} N_l^m P_l^m(\cos\theta) \right] \quad (2)$$

where $l_{\max}$ denotes the *series degree* which controls the accuracy of the approximation, and $\mathbf{a} = (a_0^0, ..., a_{l_{\max}}^{l_{\max}})^T$ and $\mathbf{b} = (b_1^1, ..., b_{l_{\max}}^{l_{\max}})^T$ denote the expansion coefficient vectors. A specific 3D shape can be described by adjusting $\mathbf{a}$ and $\mathbf{b}$.

## 2.2 3D Parametric Intensity Model

To model the imaging process and to incorporate the effect of the point spread function (PSF) into (2), we use a convolution by a Gaussian kernel. The 3D SH intensity model is then given by

$$g_{\mathrm{SH}}(\mathbf{x}) = \Phi_\sigma(r + r_{\mathrm{SH}}(\pi - \theta, \varphi + \pi)) - \Phi_\sigma(r - r_{\mathrm{SH}}(\theta, \varphi)) \quad (3)$$

where $\Phi_\sigma$ is the Gaussian error function with standard deviation $\sigma$. To evaluate the model at position $\mathbf{x} = (x, y, z)^T$ in Cartesian coordinates, the spherical parameters $r$, $\theta$, and $\varphi$ are computed by $r(\mathbf{x}) = \sqrt{x^2 + y^2 + z^2}$, $\theta(\mathbf{x}) = \cos^{-1}\left(\frac{z}{r(\mathbf{x})}\right)$, and $\varphi(\mathbf{x}) = \tan^{-1}\left(\frac{y}{x}\right)$. We further include a 3D rigid transform $\mathcal{R}(\mathbf{x}, \mathbf{x}_0, \boldsymbol{\alpha})$ with translation $\mathbf{x_0} = (x_0, y_0, z_0)^T$ and rotation $\boldsymbol{\alpha} = (\alpha, \beta, \gamma)^T$ as well as background and foreground intensity levels $a_0$ and $a_1$ to obtain the final 3D SH intensity model

$$g_{\mathrm{M,SH}}(\mathbf{x}, \mathbf{p}) = a_0 + (a_1 - a_0) g_{\mathrm{SH}}(\mathcal{R}(\mathbf{x}, \mathbf{x}_0, \boldsymbol{\alpha})) \quad (4)$$

where $\mathbf{p} = (\mathbf{a}, \mathbf{b}, a_0, a_1, \sigma, \boldsymbol{\alpha}, \mathbf{x_0})^T$ denotes the model parameter vector.

## 2.3 Automatic 3D Foci Segmentation

For automatic segmentation of 3D fluorescent foci, we propose a two-step approach. In the first step, initial center positions of different foci are determined using a 3D Gaussian filter for noise reduction followed by background suppression and 3D local maxima search for each individual cell nucleus. In the second step, the 3D SH intensity model (4) is applied to the 3D position of each local maximum. To fit the model to the 3D image data, a least-squares intensity-based optimization is performed within a spherical region of interest. For the optimization, we use the method of Levenberg and Marquardt which incorporates first order partial derivatives of $g_{\mathrm{M,SH}}$ w.r.t. the model parameters. Note that all partial derivatives of $g_{\mathrm{M,SH}}$ can be derived analytically.

## 3   Results

We have successfully applied our approach to 33 3D confocal microscopy images of mouse fibroblast cells ($130 \times 130 \times 41$ or $250 \times 250 \times 64$ voxels). For comparison, we also applied two previous approaches: An approach based on a 3D Gaussian intensity model [4] and a 3D combined approach based on region-adaptive segmentation and a 3D Gaussian intensity model [5]. As an example, Fig. 2 shows 3D foci segmentation results of the heterochromatin protein $1\alpha$ (HP1$\alpha$). It can be seen that for small foci the previous approach based on the 3D Gaussian model yields relatively good results, however, it fails to accurately segment large foci of irregular shape (see the yellow circles in Fig. 2b). The 3D combined approach generally yields a good result, however, for large foci of irregular shape with other foci in close proximity, undersegmentation occurs (see the yellow circle in Fig. 2c). In comparison, the new approach yields a better result (e.g., undersegmentation does not occur) and the approach can cope well with foci of different size and highly irregular shape (Fig. 2d). 3D visualizations of the segmentation result for several foci are shown in Fig. 1c.
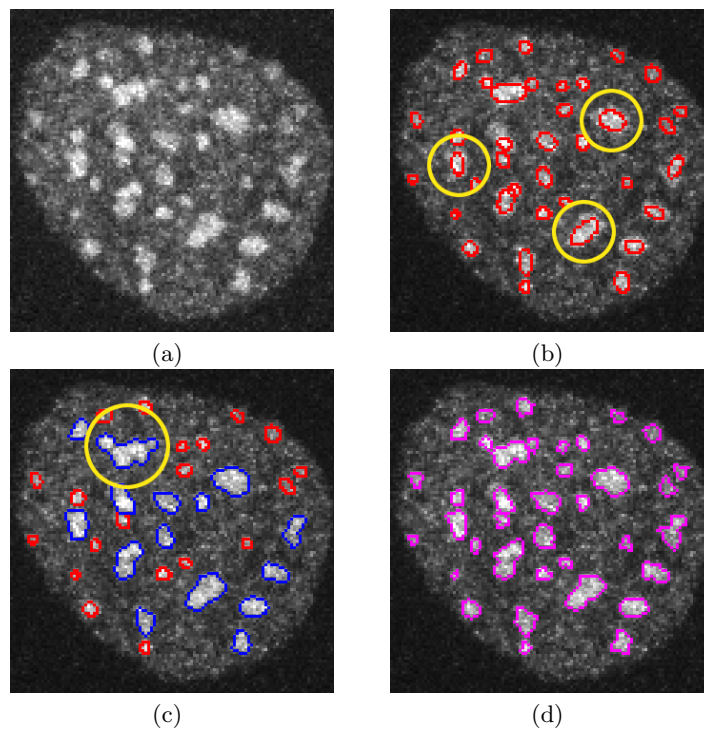


**Fig. 2.** MIP of (a) a cell nucleus in a 3D microscopy image and 3D foci segmentation results: (b) 3D Gaussian intensity model (red), (c) 3D combined approach based on region-adaptive segmentation (blue) and a 3D Gaussian intensity model (red), and (d) 3D SH intensity model (magenta).

**Table 1.** Quantitative results for real 3D microscopy image data: Mean value $\overline{D}$ and standard deviation $\sigma_D$ of the Dice coefficient for manual segmentation and automatic segmentation based on a 3D Gaussian intensity model, a 3D combined approach based on region-adaptive segmentation and a 3D Gaussian intensity model, and the 3D SH intensity model.

|  | Manual | 3D Gaussian | 3D combined | 3D SH |
|---|---|---|---|---|
| $\overline{D}$ | **0.694** | 0.651 | 0.682 | **0.714** |
| $\sigma_D$ | 0.054 | 0.111 | 0.105 | 0.098 |

To quantify the segmentation accuracy, we computed the Dice coefficient $D$ between the 3D segmentation results and 3D ground truth data. Ground truth was provided manually by an expert observer for 3D foci in seven 3D microscopy images (7 cell nuclei, 75 foci in total). To determine the interobserver variability, a second observer manually performed 3D segmentation. For the automatic approaches, all foci were segmented using a fixed set of parameters. Table 1 shows the mean value $\overline{D}$ and standard deviation $\sigma_D$ of the Dice coefficient for the different approaches for all 75 foci. It can be seen, that the new approach outperforms the two previous approaches. In addition, it turns out that the results of the new approach is comparable to manual segmentation (see the bold numbers in Table 1).

## 4  Discussion

We introduced a 3D model-based approach for automatic segmentation of 3D fluorescent heterochromatin foci. Our approach is based on a new 3D parametric intensity model using spherical harmonics (SH) and yields an analytic description of the segmented foci. Experiments using real 3D microscopy images show that the approach can cope well with foci of highly irregular shape and yields better results than two previous approaches. In future, we plan to apply our approach to a larger number of 3D images.

## References

1. Ivashkevich AN, Martin OA, Smith AJ, Redon CE, Bonner WM, Martin RF, et al. H2AX foci as a measure of DNA damage: A computational approach to automatic analysis. Mutat Res. 2011;711(1-2):49–60.
2. Dzyubachyk O, Essers J, van Cappellen WA, Baldeyron C, Inagaki A, Niessen WJ, et al. Automated analysis of time-lapse fluorescence microscopy images: from live cell images to intracellular foci. Bioinformatics. 2010;26(19):2424–2430.

3. Thomann D, Rines DR, Sorger PK, Danuser G. Automatic fluorescent tag detection in 3D with super-resolution: application to the analysis of chromosome movement. J of Microscopy. 2002;208:49–64.

4. Wörz S, Sander P, Pfannmöller M, Rieker RJ, Joos S, Mechtersheimer G, et al. 3D Geometry-Based Quantification of Colocalizations in Multichannel 3D Microscopy Images of Human Soft Tissue Tumors. IEEE Trans on Medical Imaging. 2010;29(8):1474–1484.

5. Eck S, Rohr K, Müller-Ott K, Rippe K, Wörz S. Combined Model-Based and Region-Adaptive 3D Segmentation and 3D Co-Localization Analysis of Heterochromatin Foci. In: Proc. Workshop Bildverarbeitung für die Medizin (BVM'12). Informatik aktuell. Berlin, Germany; 2012. p. 9–14.

6. Székely G, Kelemen A, Brechbühler C, Gerig G. Segmentation of 2-D and 3-D objects from MRI volume data using constrained elastic deformations of flexible Fourier contour and surface models. Medical Image Analysis. 1996;1(1):19–34.

7. Arfken GB, Weber HJ, Harris FE. Mathematical Methods for Physicists. Sixth ed. Academic Press; 2005.

8. El-Baz A, Nitzken M, Khalifa F, Elnakib A, Gimel'farb G, Falk R, et al. 3D Shape Analysis for Early Diagnosis of Malignant Lung Nodules. In: Proc. 22nd Internat. Conf. on Information Processing in Medical Imaging (IPMI'11). vol. 6801 of Lecture Notes in Computer Science; 2011. p. 772–783.

9. Shen L, Firpi HA, Saykin AJ, West JD. Parametric surface modeling and registration for comparison of manual and automated segmentation of the hippocampus. Hippocampus. 2009;19(6):588–595.

10. Baust M, Navab N. A Spherical Harmonics Shape Model for Level Set Segmentation. In: Proc. 11th European Conference on Computer Vision. vol. 6313 of Lecture Notes in Computer Science. Springer Berlin Heidelberg; 2010. p. 580–593.